Physica B 513 (2017) 62–68

Contents lists available at ScienceDirect

Physica B

journal homepage: www.elsevier.com/locate/physb

Defect concentration in nitrogen-doped graphene grown on Cu substrate: A thickness effect

Dhananjay K. Sharma[a,b,*], Sara Fateixa[c], María J. Hortigüela[b], Reddithota Vidyasagar[a], Gonzalo Otero-Irurueta[b], Helena I.S. Nogueira[c], Manoj Kumar Singh[b], Andrei Kholkin[a,d,**]

[a] Department of Physics & CICECO – Aveiro Institute of Materials, University of Aveiro, 3810-193 Aveiro, Portugal
[b] Department of Mechanical Engineering & Centre for Mechanical Technology & Automation, University of Aveiro, 3810-193 Aveiro, Portugal
[c] Department of Chemistry & CICECO – Aveiro Institute of Materials, University of Aveiro, 3810-193 Aveiro, Portugal
[d] School of Natural Sciences and Mathematics, Ural Federal University, 620000 Ekaterinburg, Russia

ARTICLE INFO

Keywords:
Graphene
CVD
High Resolution-X-ray Photoelectron Spectroscopy (HR-XPS)
Raman
Defects
Nitrogen-doping

ABSTRACT

Tuning the band-gap of graphene is a current need for real device applications. Copper (Cu) as a substrate plays a crucial role in graphene deposition. Here we report the fabrication of *in-situ* nitrogen (N) doped graphene via chemical vapor deposition (CVD) technique and the effect of Cu substrate thickness on the growth mechanism. The ratio of intensities of *G* and *D* peaks was used to evaluate the defect concentration based on local activation model associated with the distortion of the crystal lattice due to incorporation of nitrogen atoms into graphene lattice. The results suggest that Cu substrate of 20 μm in thickness exhibits higher defect density (1.86×10^{12} cm^{-2}) as compared to both 10 and 25 μm thick substrates (1.23×10^{12} cm^{-2} and 3.09×10^{11} cm^{-2}, respectively). Furthermore, High Resolution -X-ray Photoelectron Spectroscopy (HR-XPS) precisely affirms ~0.4 at% of nitrogen intercalations in graphene. Our results show that the substitutional type of nitrogen doping dominates over the pyridinic configuration. In addition, X-ray diffraction (XRD) shows all the XRD peaks associated with carbon. However, the peak at ~24° is suppressed by the substrate peaks (Cu). These results suggest that nitrogen atoms can be efficiently incorporated into the graphene using thinner copper substrates, rather than the standard 25 μm ones. This is important for tailoring the properties by graphene required for microelectronic applications.

1. Introduction

Theoretically' graphene was studied for a long time and it was believed that the isolation of monolayer materials at finite temperatures is unphysical due to inherent thermodynamic instabilities of their lattices. Novoselov et al. [1] in 2004, used mechanical exfoliation method to rediscover graphene which became a promising electronic material, due to its unique properties such as high electron mobility useful for several potential applications [2–7]. However, to realize the graphene-based circuits in real devices, the modulation of electronic properties of this material is required. One way to achieve this is to induce defects by doping with n- or p-type doping elements. Previously reports show that carbon nanotubes (CNTs) can be efficiently doped with n-type and p-type using nitrogen and boron atoms, respectively [8–10]. In case of graphene, doping can also significantly change its electronic properties. Theoretical and experimental studies [11] revealed that substitutional doping should modify the electronic band structure of graphene [12–14] which enhances the possibilities of its applications [15–17]. Doped graphene promises several breakthroughs and widespread potential applications due to predicted superconductivity [18], ferromagnetism [19], etc. In view of this, intensive research is now focusing on the possibility of graphene doping under controlled conditions.

There are various methods to produce graphene such as mechanical exfoliation [1], thermal decomposition of silicon carbide (SiC) [20], oxidation of graphene [21], liquid-phase exfoliation of graphite [22], Chemical Vapor Deposition (CVD) [23] etc. Out of them, for the large-scale industrial growth of graphene, CVD-based fabrication methods are preferred. Different substrates were used to synthesize graphene by CVD. A variety of transition metals such as ruthenium (Ru) [24,25], iridium (Ir) [26,27], cobalt (Co) [28], nickel (Ni) [29,30], platinum (Pt) [28,31] and palladium (Pd) [28,32] are being extensively used for the graphene growth. The carbon solubility in metals and the growth conditions determine the deposition mechanism and also define the

* Corresponding author at: Department of Physics & CICECO – Aveiro Institute of Materials, University of Aveiro, 3810-193 Aveiro, Portugal.
** Corresponding author at: School of Natural Sciences and Mathematics, Ural Federal University, 620000 Ekaterinburg, Russia.
E-mail addresses: dhananjay@ua.pt (D.K. Sharma), kholkin@ua.pt (A. Kholkin).

http://dx.doi.org/10.1016/j.physb.2017.03.004
Received 6 February 2017; Accepted 1 March 2017
Available online 02 March 2017

morphology along with the thickness of the graphene films. Graphene grown on Co(0001) and Ni(111) surfaces has a lattice mismatch of less than 1% [26], whereas it can be more than 1% in the case of Pt(111) [28], Pd(111) [28], Ru(111) [25], and Ir(111) [27].

Ni and Cu substrates are the most widely used due to low cost and availability. Kim et al. reported high optical transparency (80%), low sheet resistance and greater electron mobility of 3700 cm^2/V s for the graphene grown by CVD on polycrystalline Ni, and transferred on to SiO_2 substrate [33]. Recently, Li et al. have demonstrated that Ni limits the control of the number of layers, resulting in a single to a few layer graphene [34]. In the case of Cu, graphene grows as uniform and high-quality single layer over a large area. The studies of Sutter et al. have demonstrated uniform high quality single layered graphene growth over a large area up to 30-in. on polycrystalline substrates [35]. Their study further confirmed 95% of the copper surface covered by a single layered graphene while the remaining area was covered by 2–3 layer graphene. Copper, as a substrate, has shown catalyzing behavior for several carbon allotropes, such as graphite [36], diamond [37], carbon nanotubes [38,39] and graphene [35], as was unintentionally achieved in 1991 in an experiment designed to catalyze the growth of diamond by CVD.

Given the extensive applications of graphene related materials and based on the success of graphene growth on the large areas of Cu substrates, we aimed to grow doped thin films by CVD. We performed the growth of highly homogenous *in-situ* nitrogen doped graphene on large Cu substrates in its single layer form. The effect of substrate thickness on defect structure is studied by calculating defect concentrations based on local activation model associated with the distortion of the crystal lattice upon introduction of nitrogen atoms. By means of confocal Raman spectroscopy and XPS we further confirmed the existence of defects created by nitrogen atoms on the different Cu substrates. Our studies reveal that graphene grown on 20 μm thick Cu exhibits higher concentration of defects, as compared to both 10 and 25 μm substrates.

2. Experimental

2.1. Growth of N-doped Graphene by CVD

Graphene was grown on 10, 20 and 25 μm thick copper substrates (GoodFellow, 99.97+%). Ammonia (NH_3) gas was used *in-situ* to supply nitrogen atoms during growth in a chemical vapor deposition system (CVD) with an alumina tube furnace, (see the schematic diagram). To clean the Cu substrates, they were annealed at 900 °C for 60 min under hydrogen (H_2) atmosphere at 85 standard cubic centimeters per minute (sccm). This procedure also increases the grain size of the copper and removes the copper oxide. After annealing, the furnace temperature was slowly increased from 900 to 980 °C. Ammonia along with methane (CH_4) and H_2 were flowed into the furnace for a period of 15 min with the flow rate of CH_4:H_2:NH_3: 10:51:10 sccm. After 15 min NH_3 flow was discontinued, while methane and hydrogen were continued for 20 min more with the flow rate of CH_4:H_2:10:51 sccm. Upon this, the samples were rapidly cooled down to room temperature and taken out. All growth experiments were performed at pressure of 35 Torr.

2.2. High Resolution X-Ray Diffraction

The crystal structure of all the films was determined by measuring the high resolution X-ray diffraction (grazing incidence, 0.5°) acquired with a Rigaku Geigerflex diffractometer with Cu K_α radiation (λ=1.5418 Å) in the 2θ range 5–80°.

2.3. Raman spectroscopy

N-doped graphene thin films were characterized by Raman spectroscopy using a combined Raman-AFM-SNOM confocal microscope (alpha 300 RAS+, WITec, Germany). He:Ne laser operating at 633 nm and Nd:YAG laser operating at 532 nm were used as excitation sources. The power of the laser was varied from 0.5 to 5 mW, in order not to damage/heat the sample. Raman imaging experiments were performed by raster-scanning the laser beam over the samples and accumulating the full Raman spectra at each pixel. Raman images were constructed by integrating over specific Raman bands using WITec software for data evaluation and processing.

2.4. High-Resolution X-Ray Photoelectron Spectroscopy

High-Resolution X-Ray Photoelectron Spectroscopy was performed with an Ultra High Vacuum (UHV) system using a base pressure of 2×10^{-10} mbar. The system was equipped with a hemi-spherical electron energy analyser (SPECS Phoibos 150), a delay-line detector and a monochromatic AlK_α (λ=1486.74 eV) X-ray source. High resolution spectra were recorded at normal emission take-off angle and with a pass-energy of 20 eV, which provides an overall instrumental peak broadening of about 0.5 eV.

3. Results and discussion

3.1. X-ray diffraction

HR-XRD (θ–2θ) scans of nitrogen doped graphene grown on different Cu substrates are depicted in Fig. 1. XRD patterns of Cu substrate before and after deposition of nitrogen doped graphene on 10, 20 and 25 μm thick substrates can be seen in the Figure. The results show the presence of strong peaks associated with Cu which suppresses the carbon (graphene) peak, typically expected around $2\theta \sim 24°$. This could be due to the fact that only a few layer graphene was grown on the substrate, such observation being reported in literature for graphene films on various metal substrates. Based on our XRD results three distinct diffraction peaks are defined at approximately $2\theta \sim 43°$, 50°, and 74°, which correspond to (003), (202) and (220) reflections of carbon [40] and the crystallographic plane of Cu (111), (200) and (220), respectively [41]. The absence of other peaks confirms that no other elements are present in our sample as an impurity.

3.2. Raman spectroscopy and defect calculation

Raman spectroscopy is the best fingerprint technique for analyzing the properties of the carbon related materials including graphene [42]. This technique allows distinguishing among single layer, a few layer graphene and thick graphite. It is also sensitive to defects, excess charge, strain and atomic arrangement of the edges. Fig. 2 shows the

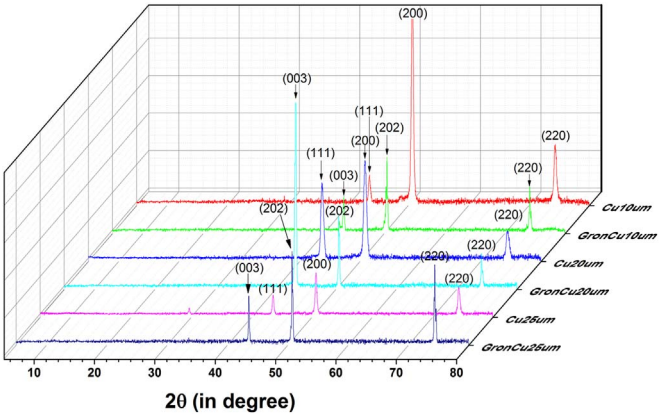

Fig. 1. XRD patterns with corresponding peaks of Cu substrate (before deposition) and after deposition of nitrogen doped graphene.

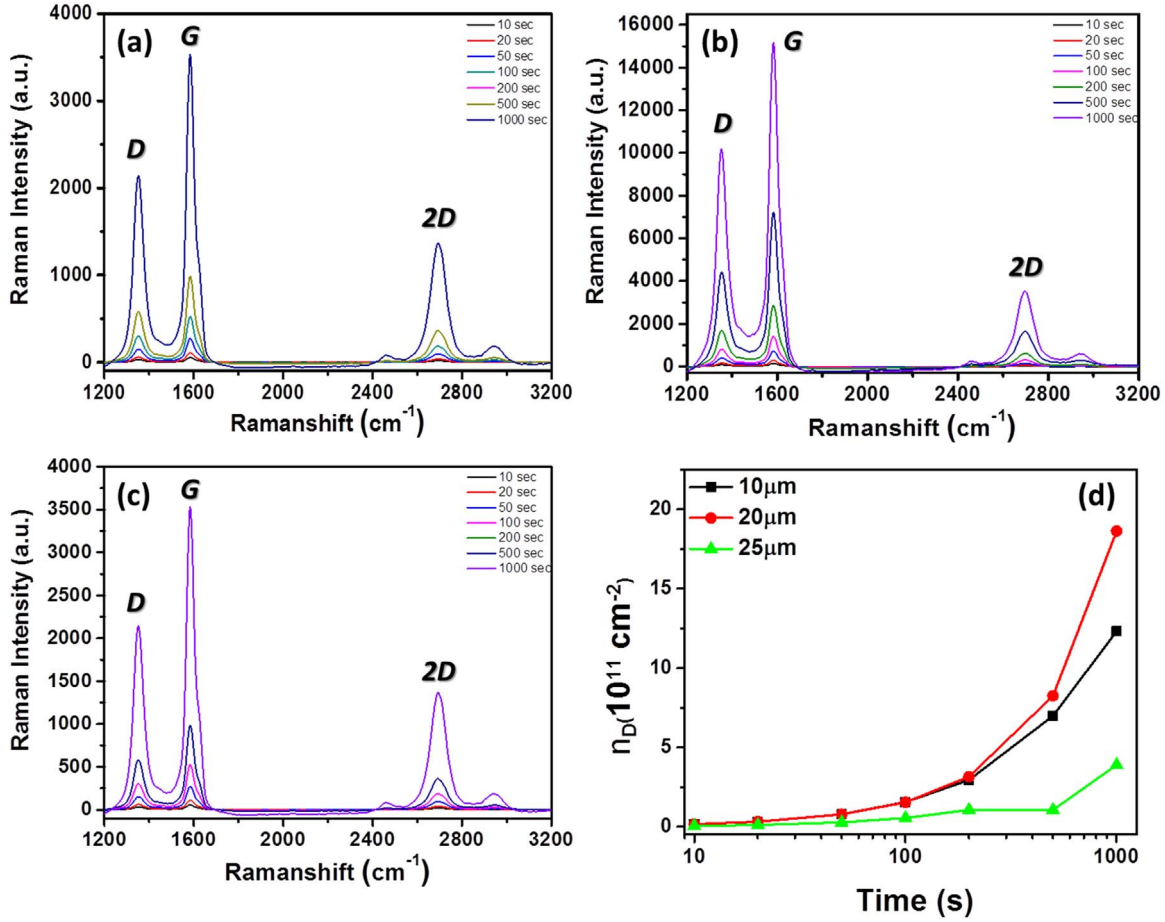

Fig. 2. Raman spectra of graphene grown on (a) 10 μm, (b) 20 μm and (c) 25 μm thick Cu substrates showing distinct *D*, *G* and *2D* peaks. (d) Defect density as a function of acquisition time for the graphene grown on 10 μm (squares), 20 μm (circles) and 25 μm (triangles) thick Cu substrates.

Raman spectroscopy results of nitrogen doped graphene grown on 10, 20 and 25 μm thick Cu substrates. The spectra were recorded at different time intervals in the range from 10 to 1000 s. The peak intensities related to *D*, *G*, *D′* and *2D* features were collected and fitted with Lorentzian functions. As widely accepted we refer to their heights as peak intensities and these are denoted as I_D, I_G, $I_{D'}$, I_{2D} for the *D*, *G*, *D′*, and *2D* peaks, respectively.

G and *2D* peaks must satisfy the Raman selection rule and this makes Raman spectroscopy one the most important tools for probing the structural defects. The first two peaks are activated by single-phonon intervalley and intravalley scattering processes, and the defect peaks *D* and *D′* provide the missing momentum in order to satisfy the momentum conservation in the Raman scattering process [43,44]. In our case the *D* peak was found almost in the same position in all the samples (~1354 cm^{-1}). However, the values of FWHM were found to be around 43, 53 and 53 cm^{-1} for 10, 20 and 25 μm thick substrates, respectively. This band originates from the breathing modes of six-membered rings that are activated by defects. The *G* peak was found to be at ~1583 cm^{-1} (FWHM ~47 cm^{-1}), ~1584 cm^{-1} (FWHM ~45 cm^{-1}) and ~1585 cm^{-1} (FWHM ~42 cm^{-1}) for 10, 20 and 25 μm thick Cu substrates, respectively, which are due to the E_{2g} phonon at the Brillouin zone center. Finally, *2D* peaks at ~2694 cm^{-1} (FWHM ~63 cm^{-1}), ~2697 cm^{-1} (FWHM ~100 cm^{-1}) and ~2695 cm^{-1} (FWHM ~87 cm^{-1}) for 10, 20 and 25 μm thick Cu substrates, respectively, are assigned to the second orders of *D* peak. All these values were acquired at 100 s acquisition time during Raman measurements. Lucchese et al. [45] have made extensive efforts to study the relationship between the amount (and nature) of defects and the intensities of *D* and *D′* peaks. A simple formula was proposed to calculate the defect density n_D (in cm^{-2}) with the help of mean distances in graphene (L_D, nm) with relation to I_D/I_G.

$$\frac{I_{(x)}}{I_{(G)}} = C_A \frac{r_A^2 - r_S^2}{r_A^2 - 2r_S^2} \left[e^{\frac{-\pi r_S^2}{L_D^2}} - e^{\frac{-\pi(r_A^2 - r_S^2)}{L_D^2}} \right] \quad (1)$$

where $x = D$ or D'; r_S (1 nm) and r_A (3.1 nm) are the radii of the "structurally disordered" area and the "activated area" around the defects, respectively [45].

C_A correlates with the electron-phonon matrix elements and it was found to be 4.2 using the green laser excitation (532 nm). From the above equation, the defect densities n_D (in cm^{-2}) were calculated as follows:

$$n_D = 10^{14} / \pi L_D^2 \quad (2)$$

Fig. 2(d) presents the defect densities calculated for the substrates with different thicknesses. From the measured spectra it was concluded that the highest defect density is observed for 20 μm thick Cu substrate. Possible reason for this effect could be the increased surface roughness due to rolling process used for the commercial fabrication of Cu substrates [46]. Due to the strong *D* peak seen in 20 μm Cu substrate and because of the defect density, the "activated" area starts to coalesce and the structurally disordered area dominates in the graphene sheets [47]. Fig. 2(d) summarizes the defect densities calculated with different laser acquisition times in the range 10 – 1000 s. To check the homogeneity of the samples, we performed Raman mapping. Fig. 3 shows the Raman maps of the *G* band and *D* band intensities, as well as intensity of *2D* band of the graphene grown on 10, 20 and 25 μm thick substrates. The contrast was more or less uniform signifying that the graphene was homogeneously deposited on Cu, though the quality

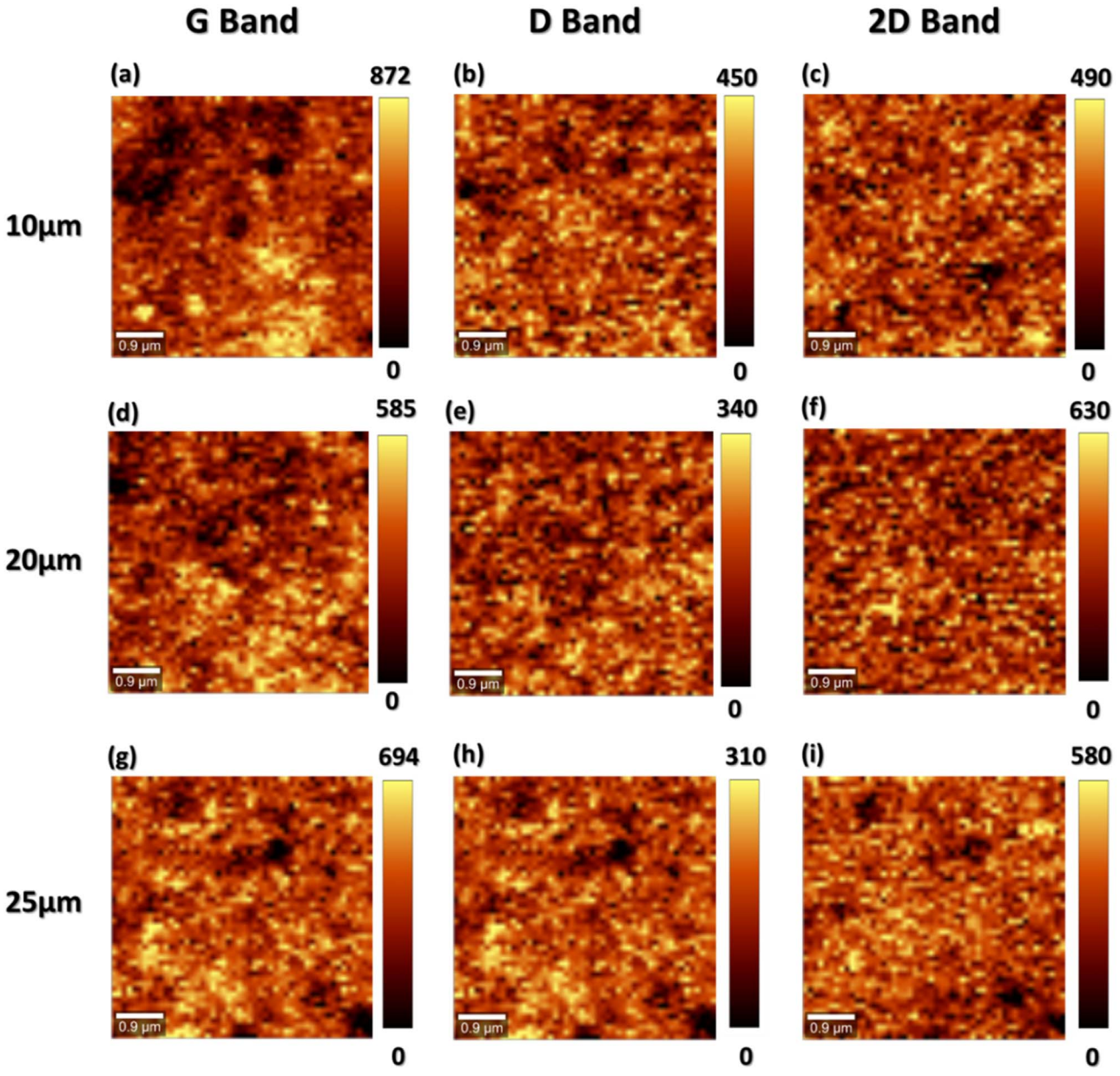

Fig. 3. Raman images (532 nm laser source) using the integrated intensities of the *G* band, *D* band and *2D* band of graphene grown on 10 µm, 20 µm and 25 µm thick Cu substrates, respectively. The vertical bars show the color profile in the Raman images, with scale in CCD counts.

differs due to different quality of substrates used during experiment. The mapping also confirms the overall wide spread deposition of nitrogen doped-graphene on over most of the substrate surface. This result suggests that the CVD process is able to produce sufficiently large areas of graphene.

3.3. High-Resolution X-Ray Photoelectron Spectroscopy

Furthermore, we performed HR-XPS to re-confirm the amount of defects created by doping in graphene. XPS is a well-established technique used for revealing the elemental composition and the chemical environment of the detected elements. Fig. 4(a) shows the overview spectra of as grown N doped graphene on 10, 20 and 25 µm thick substrates, while Fig. 4(b, c) depicts the carbon (C) 1 s and nitrogen (N) 1 s core levels, respectively.

C 1 s core level (Fig. 4(b)) can be fitted by a single component, centered at a BE of 284.5 eV, ascribed to C sp^2 [48]. Thus, from the XPS point of view C 1 s seems to be almost equal in all the samples. On the contrary, significant changes were detected in the N 1 s core level (Fig. 4(c)). Under the same growing conditions the quantity of nitrogen is almost zero in the case of the 25 µm copper substrate (bottom spectra). The blue dashed line that is included in the bottom spectra is only a guide for the eye, fixed at the BE that we could expect substitutional nitrogen in graphene. On the other hand, the nitrogen intercalation in the graphene sheets is clear in the upper spectra, corresponding to the sample grown on a 20 µm thick copper substrate. Two components are clearly distinguished in the respective spectrum of N 1 s core level. The first one, centered at BE of 401.7 eV, is ascribed to substitutional nitrogen atoms in a graphene sheet, whereas the second component (BE =398.5 eV) is attributed to nitrogen atoms in a pyridinic configuration [11]. In this sample the amount of nitrogen quantified by XPS is about 0.4 at%. Finally, in the case of the sample grown on 10 µm thick copper substrate a sharp N peak is detected at 396.7 eV. This value of BE is too low for the substitutional nitrogen in the graphene sheet. On the contrary, it can be related to the atomic nitrogen bonded to the copper substrate [49]. Fig. 5(b) shows the

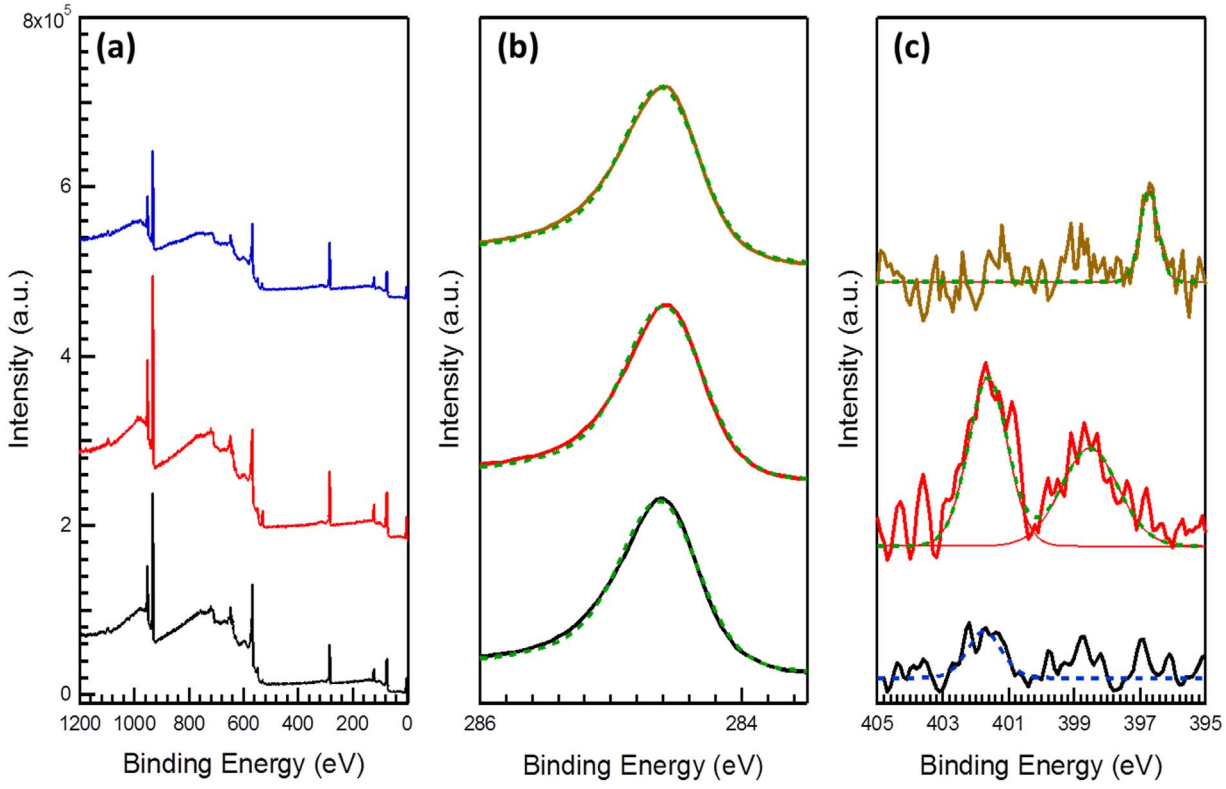

Fig. 4. HR-XPS comparison of nitrogen doped graphene grown on Cu substrates of 10 (brown curves), 20 (black curves) and 25 μm (red curves). (a) Overview spectra of N-doped graphene. (b) C 1 s and (c) N 1 s core levels. The best fits are shown as green dotted line. For N 1 s spectra of graphene grown on 25 μm Cu substrate (bottom spectra) the blue line is a guide for the eyes. (For interpretation of the references to color in this figure legend, the reader is referred to the web version of this article)

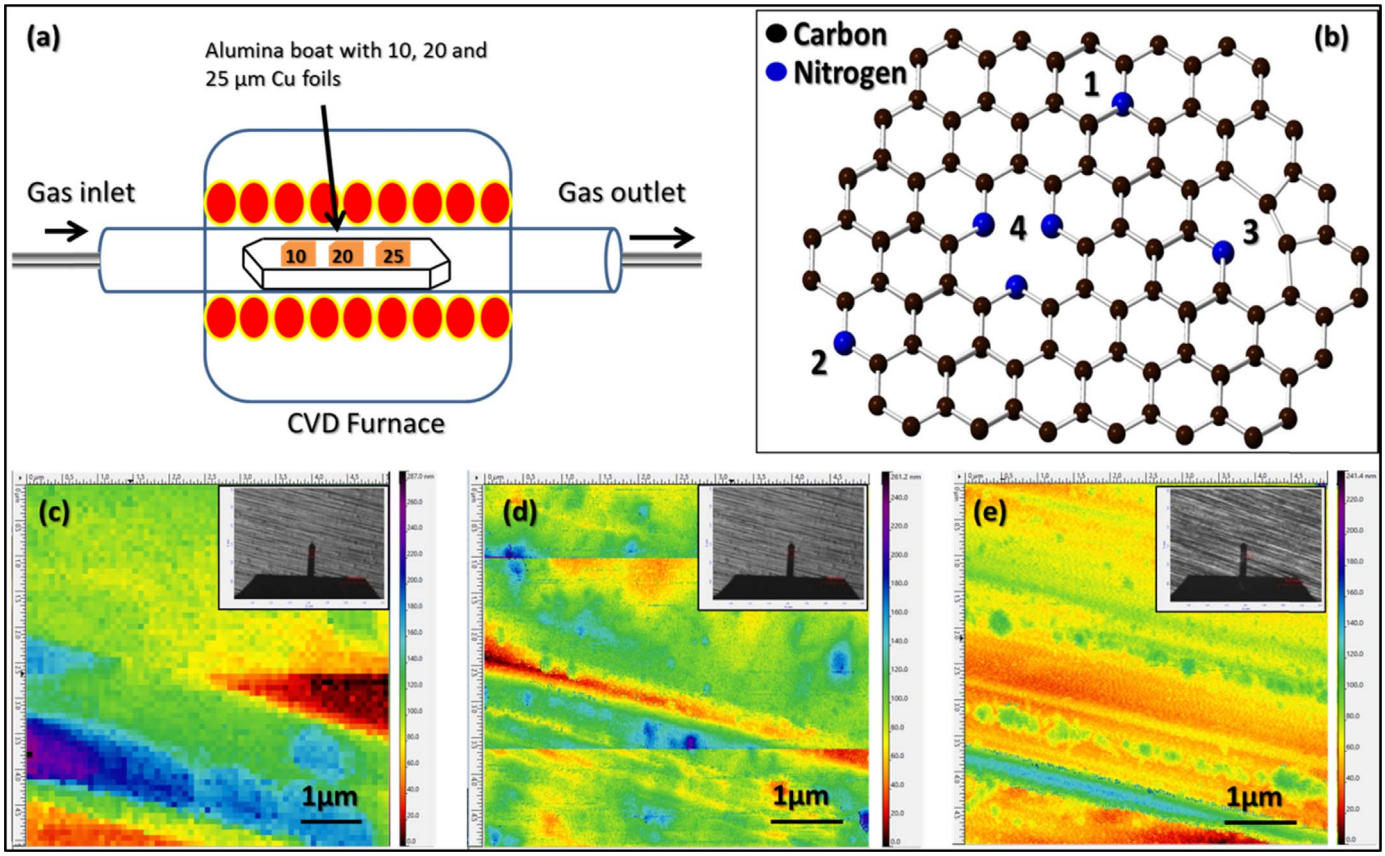

Fig. 5. (a) Schematic diagram of the experiment showing the 10, 20 and 25 μm Cu substrates placed in alumina boat in CVD furnace, (b) Possible nitrogen incorporation in graphene structure showing (1) substitutional or graphitic N, (2) pyridine-like N, (3) single N pyridinic vacancy, (4) triple N pyridinic vacancy, (c–e) Atomic Force Microscopy images for average RMS surface of virgin Cu subtrates of 10, 20 and 25 μm thickness, respectively (inset shows the optical image captured during AFM aquisition).

possible sites for N intercalation in graphene sheets. There are mainly three types of bonding found in graphene with incorporated nitrogen, namely, substitutional, pyridinic and pyrrolic ones. However, in our graphene (grown on a 20 μm thick copper) we found only substitutional and pyridinic configurations of bonding. In substitutional type of configuration, three nitrogen valence electron form three σ– bonds, one electron fills the π–states, and the fifth electron enters the π*–states of the conduction band, providing a strong doping effect.

3.4. Surface analysis

Commonly, 25 μm Cu substrates are the ones mostly used for the deposition of graphene. In our experiment, we used three thicknesses of 10, 20 and 25 μm and studied their effect on the nitrogen incorporation. As discussed above, we found that 20 μm Cu substrates are the best for graphene doping. This thickness provides the highest defect concentration as compared to 10 and 25 μm thicknesses. The conceivable mechanism can be as follows: it is well known that Cu sheets are prepared using a rolling process. This rolling technique creates lines with sufficiently high roughness (average roughness of highly smooth Cu sheet can be as high as 100 nm) [46]. Since Cu surface plays an important and crucial role for grain growth during annealing process (during deposition) [50], we infer that, in principle, thinner Cu substrates are likely to have higher surface roughness that will create more nucleation sites for graphene growth and its subsequent doping. As in the case of 20 μm foil, the results show that it is quite possible that the number of grains could be higher than that for 25 μm substrates. It is conceivable that 10 μm substrate might have even more grains available for nucleation as compared to 20 and 25 μm Cu substrates but, since the deposition is done around 1000 °C, it leads to strong evaporation of Cu atoms from Cu surface (because of the melting temperature of Cu ~1085 °C). This is deleterious for the graphene deposition and its doping. It is worth mentioning that we tried the same experiment around ~1050 °C and it was surprising that 10 μm Cu substrate was completely evaporated due to high temperature, as also confirmed by Ago et al. [50]. Therefore, 20 μm seems to be optimal thickness for efficient defect incorporation as compared to 10 and 25 μm thick foils.

Atomic Force Microscopy (AFM) technique was used to quantify the root mean square (RMS) roughness of virgin Cu foils in a semicontact mode using a Si cantilever with the force constant 3 Nm^{-1} . The results are presented in Fig. 5(c-e). The Cu substrates with uniform thickness of 10, 20, and 25 μm have an average RMS roughness of 46, 25 and 18 nm, respectively. Hence, from the above observation we infer that thinner Cu substrates having higher roughness as compared to thicker substrates; consequently, the roughness is probably responsible for a number of grains available of nucleation of graphene.

4. Conclusions

In conclusion, we observed the apparent effect of Cu substrate thickness on in-situ nitrogen doping of graphene by using NH_3 as a precursor. 25 μm thick Cu foils are the standard substrates which were extensively used as substrates for the growth of pristine epitaxial graphene. Our results based on Raman spectroscopy, HR-XPS, HR-XRD and AFM indicate that the use of a thinner copper substrate (20 μm) rather than the standard one (25 μm) is a means to significantly increase the efficiency of doping of graphene sheets with nitrogen. Thus this study provides a clue for heteroatom engineering of graphene, which is required for the electronic applications of graphene.

Acknowledgments

DKS acknowledges Svaagata Erasmus Mundus for financial support for a PhD fellowship. S. Fateixa and R. Vidyasagar thank Fundação para a Ciência e Tecnologia (FCT) for the grants SFRH/BPD/93547/2013. and SFRH/BPD/104887/2014, respectively. AK is grateful to the Russian Foundation for Basic Research (grant No 16-29-14050-ofr-m) and Government of the Russian Federation (Act 211, Agreement 02.A03.21.0006) for the financial support. MJH acknowledges UID/EMS/00481/2013 project. G O-I thanks FCT for his investigator grant (IF/01054/2015). The work was developed within the scope of the project CICECO-Aveiro Institute of Materials, POCI-01–0145-FEDER-007679 (FCT Ref. UID/CTM/50011/2013), financed by National Funds through the FCT/MEC and, when appropriate, co-funded by FEDER under the PT2020 Partnership Agreement.

References

[1] K.S. Novoselov, A.K. Geim, S.V. Morozov, D. Jiang, Y. Zhang, S.V. Dubonos, I.V. Grigorieva, A.A. Firsov, Electric field effect in atomically thin carbon films, Science 306 (2004) 666–669.
[2] A.K. Geim, K.S. Novoselov, The rise of graphene, Nat. Mater. 6 (2007) 183–191.
[3] V.V. Cheianov, V. Fal'ko, B.L. Altshuler, The focusing of electron flow and a Veselago lens in graphene p-n junctions, Science 315 (2007) 1252–1255.
[4] H.B. Heersche, P. Jarillo-Herrero, J.B. Oostinga, L.M.K. Vandersypen, A.F. Morpurgo, Bipolar supercurrent in graphene, Nature 446 (2007) 56–59.
[5] J.R. Williams, L. DiCarlo, C.M. Marcus, Quantum Hall effect in a gate-controlled p-n junction of graphene, Science 317 (2007) 638–641.
[6] X. Li, X. Wang, L. Zhang, S. Lee, H. Dai, Chemically derived, ultrasmooth graphene nanoribbon semiconductors, Science 319 (2008) 1229–1232.
[7] D.A. Areshkin, C.T. White, Building blocks for integrated graphene circuits, Nano Lett. 7 (2007) 3253–3259.
[8] K. Xiao, Y. Liu, Pa Hu, G. Yu, Y. Sun, D. Zhu, n-type field-effect transistors made of an individual nitrogen-doped multiwalled carbon nanotube, J. Am. Chem. Soc. 127 (2005) 8614–8617.
[9] H. Terrones, M. Terrones, E. Hernández, N. Grobert, J.C. Charlier, P.M. Ajayan, New metallic allotropes of planar and tubular carbon, Phys. Rev. Lett. 84 (2000) 1716–1719.
[10] R. Czerw, M. Terrones, J.C. Charlier, X. Blase, B. Foley, R. Kamalakaran, N. Grobert, H. Terrones, D. Tekleab, P.M. Ajayan, W. Blau, M. Rühle, D.L. Carroll, Identification of electron donor states in n-doped carbon nanotubes, Nano Lett. 1 (2001) 457–460.
[11] D. Usachov, O. Vilkov, A. Gruneis, D. Haberer, A. Fedorov, V.K. Adamchuk, A.B. Preobrajenski, P. Dudin, A. Barinov, M. Oehzelt, C. Laubschat, D.V. Vyalikh, Nitrogen-doped graphene: efficient growth, structure, and electronic properties, Nano Lett. 11 (2011) 5401–5407.
[12] M. Deifallah, P.F. McMillan, F. Corà, Electronic and structural properties of two-dimensional carbon nitride graphenes, J. Phys. Chem. C 112 (2008) 5447–5453.
[13] T.B. Martins, R.H. Miwa, A.J.R. da Silva, A. Fazzio, Electronic and transport properties of boron-doped graphene nanoribbons, Phys. Rev. Lett. 98 (2007) 196803.
[14] F. Cervantes-Sodi, G. Csányi, S. Piscanec, A.C. Ferrari, Edge-functionalized and substitutionally doped graphene nanoribbons: electronic and spin properties, Phys. Rev. B 77 (2008) 165427.
[15] M. Calandra, F. Mauri, Electronic structure of heavily doped graphene: the role of foreign atom states, Phys. Rev. B 76 (2007) 161406.
[16] R. Roldán, M.P. López-Sancho, F. Guinea, Effect of electron-electron interaction on the Fermi surface topology of doped graphene, Phys. Rev. B 77 (2008) 115410.
[17] T.O. Wehling, K.S. Novoselov, S.V. Morozov, E.E. Vdovin, M.I. Katsnelson, A.K. Geim, A.I. Lichtenstein, Molecular doping of graphene, Nano Lett. 8 (2008) 173–177.
[18] B. Uchoa, A.H. Castro Neto, Superconducting states of pure and doped graphene, Phys. Rev. Lett. 98 (2007) 146801.
[19] N.M.R. Peres, F. Guinea, A.H. Castro Neto, Coulomb interactions and ferromagnetism in pure and doped graphene, Phys. Rev. B 72 (2005) 174406.
[20] C. Berger, Z. Song, X. Li, X. Wu, N. Brown, C. Naud, D. Mayou, T. Li, J. Hass, A.N. Marchenkov, E.H. Conrad, P.N. First, W.A. de Heer, Electronic confinement and coherence in patterned epitaxial graphene, Science 312 (2006) 1191–1196.
[21] D.A. Dikin, S. Stankovich, E.J. Zimney, R.D. Piner, G.H.B. Dommett, G. Evmenenko, S.T. Nguyen, R.S. Ruoff, Preparation and characterization of graphene oxide paper, Nature 448 (2007) 457–460.
[22] X. Li, G. Zhang, X. Bai, X. Sun, X. Wang, E. Wang, H. Dai, Highly conducting graphene sheets and Langmuir-Blodgett films, Nat. Nano 3 (2008) 538–542.
[23] T. Ma, W. Ren, Z. Liu, L. Huang, L.-P. Ma, X. Ma, Z. Zhang, L.-M. Peng, H.-M. Cheng, Repeated growth–etching–regrowth for large-area defect-free single-crystal graphene by chemical vapor deposition, ACS Nano 8 (2014) 12806–12813.
[24] P.W. Sutter, J.-I. Flege, E.A. Sutter, Epitaxial graphene on ruthenium, Nat. Mater. 7 (2008) 406–411.
[25] F.J. Himpsel, K. Christmann, P. Heimann, D.E. Eastman, P.J. Feibelman, Adsorbate band dispersions for C on Ru(0001), Surf. Sci. 115 (1982) L159–L164.
[26] J. Coraux, A.T. N'Diaye, C. Busse, T. Michely, Structural Coherency of Graphene on Ir(111), Nano Lett. 8 (2008) 565–570.
[27] N.A. Kholin, E.V. Rut'kov, A.Y. Tontegode, The nature of the adsorption bond between graphite islands and iridium surface, Surf. Sci. 139 (1984) 155–172.
[28] J.C. Hamilton, J.M. Blakely, Carbon segregation to single crystal surfaces of Pt, Pd

and Co, Surf. Sci. 91 (1980) 199–217.
[29] M. Eizenberg, J.M. Blakely, Carbon monolayer phase condensation on Ni(111), Surf. Sci. 82 (1979) 228–236.
[30] A. Reina, X. Jia, J. Ho, D. Nezich, H. Son, V. Bulovic, M.S. Dresselhaus, J. Kong*, Layer area, few-layer graphene films on arbitrary substrates by chemical vapor deposition, Nano Lett. 9 (2009) (3087-3087).
[31] H. Zi-Pu, D.F. Ogletree, M.A. Van Hove, G.A. Somorjai, Leed theory for incommensurate overlayers: application to graphite on Pt(111), Surf. Sci. 180 (1987) 433–459.
[32] T.A. Land, T. Michely, R.J. Behm, J.C. Hemminger, G. Comsa, STM investigation of single layer graphite structures produced on Pt(111) by hydrocarbon decomposition, Surf. Sci. 264 (1992) 261–270.
[33] K.S. Kim, Y. Zhao, H. Jang, S.Y. Lee, J.M. Kim, K.S. Kim, J.-H. Ahn, P. Kim, J.-Y. Choi, B.H. Hong, Large-scale pattern growth of graphene films for stretchable transparent electrodes, Nature 457 (2009) 706–710.
[34] A.N. Obraztsov, E.A. Obraztsova, A.V. Tyurnina, A.A. Zolotukhin, Chemical vapor deposition of thin graphite films of nanometer thickness, Carbon 45 (2007) 2017–2021.
[35] X. Li, W. Cai, J. An, S. Kim, J. Nah, D. Yang, R. Piner, A. Velamakanni, I. Jung, E. Tutuc, S.K. Banerjee, L. Colombo, R.S. Ruoff, Large-area synthesis of high-quality and uniform graphene films on copper foils, Science 324 (2009) 1312–1314.
[36] T.P. Ong, F. Xiong, R.P.H. Chang, C.W. White, Nucleation and growth of diamond on carbon-implanted single crystal copper surfaces, J. Mater. Res. 7 (1992) 2429–2439.
[37] L. Constant, C. Speisser, F. Le Normand, HFCVD diamond growth on Cu(111). Evidence for carbon phase transformations by in situ AES and XPS, Surf. Sci. 387 (1997) 28–43.
[38] W. Zhou, Z. Han, J. Wang, Y. Zhang, Z. Jin, X. Sun, Y. Zhang, C. Yan, Y. Li, Copper catalyzing growth of single-walled carbon nanotubes on substrates, Nano Lett. 6 (2006) 2987–2990.
[39] L. Ding, A. Tselev, J. Wang, D. Yuan, H. Chu, T.P. McNicholas, Y. Li, J. Liu, Selective growth of well-aligned semiconducting single-walled carbon nanotubes, Nano Lett. 9 (2009) 800–805.
[40] Inorganic Crystal Structure Database, [PDF#01-075-9130(RDB)].
[41] Inorganic Crystal Structure Database, [PDF#03-065-9743(RDB)].
[42] F. Tuinstra, J.L. Koenig, Raman spectrum of graphite, J. Chem. Phys. 53 (1970) 1126–1130.
[43] C. Thomsen, S. Reich, Double resonant Raman scattering in graphite, Phys. Rev. Lett. 85 (2000) 5214–5217.
[44] P. Venezuela, M. Lazzeri, F. Mauri, Theory of double-resonant Raman spectra in graphene: intensity and line shape of defect-induced and two-phonon bands, Phys. Rev. B 84 (2011) 035433.
[45] M.M. Lucchese, F. Stavale, E.H.M. Ferreira, C. Vilani, M.V.O. Moutinho, R.B. Capaz, C.A. Achete, A. Jorio, Quantifying ion-induced defects and Raman relaxation length in graphene, Carbon 48 (2010) 1592–1597.
[46] Z. Luo, Y. Lu, D.W. Singer, M.E. Berck, L.A. Somers, B.R. Goldsmith, A.T.C. Johnson, Effect of substrate roughness and feedstock concentration on growth of wafer-scale graphene at atmospheric pressure, Chem. Mater. 23 (2011) 1441–1447.
[47] J.-H. Zhong, J. Zhang, X. Jin, J.-Y. Liu, Q. Li, M.-H. Li, W. Cai, D.-Y. Wu, D. Zhan, B. Ren, Quantitative correlation between defect density and heterogeneous electron transfer rate of single layer graphene, J. Am. Chem. Soc. 136 (2014) 16609–16617.
[48] R. Hawaldar, P. Merino, M.R. Correia, I. Bdikin, J. Grácio, J. Méndez, J.A. Martín-Gago, M.K. Singh, Large-area high-throughput synthesis of monolayer graphene sheet by Hot Filament Thermal Chemical Vapor Deposition, Sci. Rep. 2 (2012) 682.
[49] J. Zhao, Q. Deng, A. Bachmatiuk, G. Sandeep, A. Popov, J. Eckert, M.H. Rümmeli, Free-standing single-atom-thick iron membranes suspended in graphene pores, Science 343 (2014) 1228–1232.
[50] H. Ago, Y. Ogawa, M. Tsuji, S. Mizuno, H. Hibino, Catalytic growth of graphene: toward large-area single-crystalline graphene, J. Phys. Chem. Lett. 3 (2012) 2228–2236.